coatings

MDPI

Article

Environmentally Friendly Water-Based Self-Crosslinking Acrylate Dispersion Containing Magnesium Nanoparticles and Their Films Exhibiting Antimicrobial Properties

Denisa Steinerová [1,*], Andréa Kalendová [1], Jana Machotová [1] and Marcela Pejchalová [2]

[1] Institute of Chemistry and Technology of Macromolecular Materials, Faculty of Chemical Technology, University of Pardubice, Studentská 573, CZ-532 10 Pardubice, Czech Republic; andrea.kalendova@upce.cz (A.K.); jana.machotova@upce.cz (J.M.)

[2] Department of Biological and Biochemical Sciences, Faculty of Chemical Technology, University of Pardubice, Studentská 573, CZ-532 10 Pardubice, Czech Republic; marcela.pejchalova@upce.cz

* Correspondence: steinerovadenisa@gmail.com; Tel.: +420-727-843-211

Received: 6 March 2020; Accepted: 31 March 2020; Published: 1 April 2020

Abstract: A water-based polymeric acrylate dispersion (latex) containing MgO nanoparticles, which had been added at a concentration of 1.5% (with respect to the monomers) during the preparation procedure, was investigated as an environmentally friendly binder for sanitary interior paints. The properties of this new latex were compared to those of a reference system free of the magnesium nanoparticles, synthesized by the same route, i.e., by semi-continuous emulsion polymerization. Tests were made in order to ascertain the mechanical and chemical properties, flash corrosion resistance and antimicrobial effect of the latex films. The results revealed that the new latex containing magnesium nanoparticles provided solvent-resistant coating films having pronounced antimicrobial activity against all the tested bacterial and fungal strains. The desirable antimicrobial properties can be ascribed to the sharp-edged character of magnesium nanoparticles, the peroxidation of lipids and the formation of reactive oxygen species. Moreover, no flash corrosion was formed beneath coating films containing magnesium nanoparticles, which can be attributed to the alkaline action due to the dissolution of a fraction of MgO in latex medium. The results of all of the tests provided evidence of the superiority of the polymeric dispersion with the magnesium nanoparticles to the reference system containing no nanoparticles.

Keywords: antimicrobial coating; water-based paint; environmentally friendly binder; semi-continuous emulsion polymerization; MgO nanoparticles

1. Introduction

A number of efforts are currently made to eliminate volatile organic compounds (VOC) from common use, meaning that water-based paints are coming to the fore [1–3]. The majority of water-based paints contain up to 80% water plus some organic solvents such as glycol ethers [4]. These paints are beneficial in that they are environmentally friendly, meeting both U.S. (EPA (U.S. Environmental Protection Agency)) and European (BPD (Biocidal Products Directive)) regulations requiring the VOC content to be below the limit of 350 g per liter of water [5,6]. As a drawback, however, water-based paints (during storing) and their coatings films are subject to microbial colonization, which is an effect that needs to be prevented not just because of their possible bio-deterioration associated with economic impact [7], but also from health and safety reasons, as pathogenic microorganisms can be transferred easily from coatings to humans [8,9].

Water-based acrylate dispersions (latexes) constitute a universal, high-quality and environmentally friendly option [10]. Their synthesis has been brought to a high level [11]. The drawbacks of common latex coatings such as low resistance to solvents, adhesive properties at elevated temperatures and brittleness at low temperatures are overcome by using various crosslinking strategies [12,13]. Among them, the interfacial crosslinking, using the keto-hydrazide self-crosslinking pathway, is based on a reaction of the carbonyl group (diacetone acrylamide) at the polymeric chain and a diamine (adipic acid dihydrazide (ADH)) dissolved in the aqueous phase. The advantages of this keto-hydrazide self-crosslinking include a fast reaction at normal temperatures and one-component composition [12–14].

Microbial infectious diseases are a serious health, social and economic problem that has drawn public attention worldwide as a human health threat [15]. The prevention of biofilm formation and bacterial adhesion on various materials is subject to research [16,17]. A wide selection of additives (often toxic), providing permanent protection against the adverse effects of microorganisms, exists for paints and coatings [18–20]. Antibiotics are among the most frequently used agents for this purpose. Bacteria are becoming increasingly resistant to antibiotics, however, due to the wide application of the latter; therefore, finding new alternatives to antibiotics is urgently required [21–23]. Various inorganic and organic compounds have been applied in the past, but many of them are now banned because of their environmental harmfulness and failure to meet applicable European legislation. Specifically, the European Union adopted its Directive 98/8/EC establishing a framework of rules governing the marketing of biocidal products with a view to ensuring a high degree of protection of humans and the environment. New findings stimulate additional limitations to be placed on the quantities and numbers of substances exhibiting antimicrobial effects; therefore, new alternatives to antimicrobial protection need to be sought out [17,24,25].

Nanoparticles provide new approaches to the development of antibacterial materials because metal oxide nanoparticles demonstrate the potential for reducing bacterial contamination [26–28] and, at the same time, can exert a favorable effect on the structural properties of the paint film [29,30]. MgO is an important inorganic oxide that is widely used in many industrial areas. MgO powder microparticles find a range of applications, e.g., as rubber fillers, in adhesives, cosmetic products, artificial silk and paper. This material is also added to paints where enhanced chemical resistance is desirable; it is an ingredient in anticorrosion paints that resist the effects of sea water and in waterproof paints for wood [31–34]. It has been demonstrated that MgO is harmless to human health and the environment [35–37], yet it exhibits a destructive antibacterial activity with respect to both Gram-positive and Gram-negative bacteria and even to viruses and spores [38–40].

One of the drawbacks of latex-based coatings is flash corrosion, which is a rapid, widespread corrosion occurring solely upon the application of water-based paints to metals [41]. The occurrence and development of flash corrosion are influenced by a number of factors, particularly ambient humidity and temperature during the film drying process, polymeric dispersion type, metallic surface pre-treatment, pH of the drying paint and the presence of air pollutants. The film formation of water-based paints, occurring while the water evaporates, includes the coalescence of polymeric particles, their deformation and, ultimately, diffusion of the polymeric chains of these particles [42]. If the process of water evaporation from the paint films is slowed down, e.g., by high air humidity, the coalescence is preceded by soluble iron salt transfer into the paint film. Application of the aqueous polymeric dispersion alone on a steel substrate is usually accompanied by flash corrosion observed over the entire metal area, which acquires a red-brown color. If a pigmented paint containing the same binder is used, then local, sharply bound defects develop whose size and number may depend on the paint film thickness and porosity. Flash corrosion can be efficiently counteracted by the use of inhibitors which are frequently toxic, such as sodium benzoate and sodium nitrite [43,44].

The goal of this work was to formulate a new latex binder exhibiting chemical resistance and biocidal efficiency in the paint films in which it is used. To this end, a one-component water-based polymeric dispersion was synthesized so that MgO nanoparticles were included in the polymerization system at a concentration of 1.5% with respect to the monomers used (based on solids). A reference

system possessing the same composition but with no nanoparticles (blank) was also formulated. The paint film efficiency was assessed with respect to the biocidal effect due to the presence of magnesium nanoparticles. The antimicrobial efficiency of the pigmented vs. transparent polymeric films was assessed, potential commercial biocidal product savings were estimated, and a number of additional benefits of the binder were highlighted.

2. Materials and Methods

2.1. Incoming Materials

The latexes were prepared from monomeric methyl methacrylate (MMA), *n*-butyl acrylate (BA), methacrylic acid (MAA) and diacetone acrylamide (DAAM) supplied by Sigma-Aldrich, Prague, Czech Republic. Adipic acid dihydrazide (ADH, active substance content > 98%; Sigma-Aldrich, Prague, Czech Republic) served as the crosslinking agent; Disponil FES 993 (anion-active surfactant based on sodium polyglycol ether sulfate; BASF, Chrudim, Czech Republic), as the emulsifier; ammonium persulfate (active substance content > 99.9%; Lach-Ner, Neratovice, Czech Republic), as the initiator; and nanostructural MgO with no surface treatment, particle size < 200 nm (commercial name JR-NMg30, Xuancheng Jingrui New Materials Co., Xuancheng, China), as the antimicrobial and antifungal ingredient of the latex.

2.2. Synthesis

The semi-continuous emulsion polymerization process was used to prepare two latex types: one with MgO nanoparticles added as a component of the polymerization system ("LM") and the other with an identical composition, but with no nanoparticles added ("L0"). Details of the composition are listed in Table 1. To provide well-coalesced coatings on the one hand and non-tackiness of coatings films on the other hand, the monomer proportions were selected so that the calculated glass transition temperature (T_g) of the latex polymer was around 10 °C. (Calculation was performed according to the Fox equation [45].) ADH was added to the latex after synthesis to facilitate copolymer crosslinking via DAAM carbonyl groups.

Table 1. The ratio of monomers and nanoparticles of latex systems.

Sample	1. Phase (g) MMA/BA/MAA	2. Phase (g) MMA/BA/MAA/DAAM/MgO
LM	86/106/8	78/104/8/10/6
L0	86/106/8	72/104/8/10/0

The latexes were prepared in a glass reaction vessel at a polymerization temperature of 85 °C under nitrogen by following the procedure shown in Table 2. Distilled water, emulsifier and initiator were added to the reaction vessel prior to starting the dropwise addition of the emulsion of monomers. The emulsion addition was divided into two phases. (In the course of emulsion addition, a temperature of 85 °C was maintained in the reaction vessel.) In the first phase, the emulsion was added dropwise for 60 min, followed by a 15 min period for completion of the polymerization process while maintaining a temperature of 85 °C in the polymerization system. In the second phase, the monomer emulsion was added dropwise and combined with the addition of MgO nanoparticles for the LM latex: the MgO nanoparticles were dispersed in the acrylate monomers on a T18 digital ULTRA TURRAX (IKA Works, Staufen, Germany) dispersing machine at 20,000 rpm for 30 min, followed by exposure to the action of ultrasound in a KRAINTEK K-12.F (Kraintek s.r.o., Podhájská, Slovak Republic) bath for another 30 min. All of the ingredients were then mixed together and dispersed for another 3 min. This made up the emulsion of the monomers containing MgO nanoparticles for dropwise addition to the reaction vessel. When all of the emulsion had been added, the system was allowed to stand for 120 min for completion of the polymerization process. The pH of the cold latex containing no nanoparticles was adjusted to 8.5 using 10% aqueous ammonia. This alkalinization step could be omitted for the

latex with the nanoparticles because its pH was 10.34 due to hydration of the nanostructural MgO. The self-crosslinking latex binders were obtained by mixing with a 10% aqueous solution of ADH at the molar ratio of DAAM:ADH = 2:1.

Table 2. Composition of the polymerization system.

Reactor Feed	**(g)**
Water	140.0
Disponil FES 993	1.0
Ammonium persulfate	0.8
1. Phase	**(g)**
Water	150.0
Disponil FES 993	14.8
Ammonium persulfate	0.8
Monomers	200.0
2. Phase	**(g)**
Water	250.0
Disponil FES 993	14.8
Ammonium persulfate	0.8
Monomers	200.0
Nanoparticles MgO	6.0

2.3. Description of the Self-Crosslinking Latexes

The coagulate and coarse impurity contents of the latexes were determined by sieve analysis according to ČSN 64 9008; the zeta potential and particle size were determined by the dynamic light scattering (DLS) method on a Zetasizer Nano ZS (Malvern Panalytical, Malvern, UK) [46]; pH was measured with a Mettler Toledo FiveEasy FE20 pH-meter (Merck KGaA, Darmstadt, Germany) [47]; non-Newtonian (apparent) viscosity was measured on a RotoVisco (RT10/94 viscometer (HAAKE, Vreden, Germany)) in the cone-plate arrangement of the Searle type where the bottom plate was steady and the rotor was movable, at a speed of 0–250 min^{-1}, and with a slot width of 0.05 mm, duration of 180 s, and temperature of 21 °C (held constant with a Thermo Scientific Haake A10, Thermo Fisher Scientific, Waltham, MA, State, USA); the minimum film-forming temperature (MFFT) was determined by using a MFFT-60 instrument (Rhopoint Instruments, East Sussex, UK) according to ISO 2115; the glass transition temperature (T_g) of emulsion polymers was determined using differential scanning calorimetry (DSC) on a Pyris 1 DSC (Perkin-Elmer, Waltham, MA, USA) under nitrogen, at a heating rate of 10 °C·min^{-1}, the second heating curve was used for T_g determination and the In-Can antimicrobial efficiency of the self-crosslinking dispersions was tested by using Preventol® Dipslides (LANXESS Deutschland GmbH, Cologne, Germany). The In-Can Preservation test of antimicrobial efficiency consisted of submerging the agar part of the DipSlide into the latex for 10 s, followed by incubation at 30 °C for 120 h. The result was evaluated by using standards [48].

2.4. Description of the Pigments and Fillers

The specific weights (densities) were measured on an AutoPycnometer 1320 (Micrometritics, Norcross, GA, USA). The pigment and filler properties were as follows: Blanc Fixe filler, structure: barite, artificially precipitated $BaSO_4$ crystalline powder, pH 8.5–10, density 4.502, manufacturer/supplier: Sigma-Aldrich; Litopon 30 white pigment, structure: mix of precipitated ZnS (30%) and $BaSO_4$ pigments, pH: 6–7, density: 4.360, manufacturer/supplier: 3P-CHEM s.r.o.; Omyacarb-1VA filler, structure: calcite ($CaCO_3$). pH: 9, density: 2.935, manufacturer/supplier: Omya CZ s.r.o.; Magnesium oxide nanoparticles: structure: periclase (MgO), particle size < 200 nm, pH 8–10, density 3.576, manufacturer/supplier: Xuancheng Jingrui New Materials Co.; Titanium oxide white pigment, structure: anatase (TiO_2), pH 8–10, density 3.780, manufacturer/supplier: Prechezia a.s.; Zinc

oxide (microparticles) white pigment, structure: 99.99% zincite (ZnO), pH 7–7.4, density 5.606, manufacturer/supplier: Sigma-Aldrich; Zinc oxide nanoparticles, structure: zincite (ZnO), pH 7–7.4, density 5.606, manufacturer/supplier: Sigma-Aldrich; Zinc sulfide pigment, structure: 99.99% ZnS, pH 10–10.75, density 4.104, manufacturer/supplier: Sigma-Aldrich; MicaCelia natural filler, structure: muscovite ($K_2Al_2Si_3O_{10}(OH)_2$), pH 6–7.5, density 2.699, manufacturer/supplier: Ziegler & Co. GmbH; and Magnesium carbonate filler, structure: magnesite ($MgCO_3$ powder), pH 9.5–10.5, density: 2.162, manufacturer/supplier: Lach-Ner.

2.5. Dispersing the Latexes with the Pigments and Antimicrobial Additives for Antimicrobial/Biocidal Testing

Typical pigments and fillers (Table 3) were dispersed in the latex at concentrations of 2% and 10% (*w*/*w*) for antimicrobial efficiency testing. This enabled the contribution of the filler or pigment on the final antimicrobial efficiency of the paint film to be assessed. This implies that the paints tested contained inorganic pigments and fillers with different chemical compositions and particle structures—Mg, Zn, Ti, Ca, K, Al and Ba carbonates, oxides, sulfides, sulfites and silicates.

Zinc pyrithione (summary formula $C_{10}H_8N_2O_2S_2Zn$, CAS No.: 13463-41-7, active substance content 52–56%, pH 6.5–8.5, density, 1.12 g/cm^3, manufacturer/supplier: Lonza) at 0.1–0.3% (*w*/*w*) was also dispersed in the latex in order to examine the feasibility of achieving savings of the antimicrobial additive. The dispersions were prepared by using a Heidolph RK3 stirrer (Heidolph, Germany) at 2500 rpm for 30 min, whereby adequate conditions were attained for achieving uniform dispersion and pigment bonding to the liquid phase.

2.6. Preparation of the Paint Films: Latex Application to the Substrates

The latexes were applied to glass panels with a size of 200 mm × 100 mm × 5 mm to test the physical properties, chemical resistance and mechanical resistance (adhesion) of paint films. Mechanical (impact) resistance and corrosion resistance were tested on paint films applied to cold-rolled low-carbon steel panels with a size of 152 mm × 102 mm × 0.8 mm. Both the glass and steel panels were washed and cleaned thoroughly with chloroform before the tests [49]. The liquid latexes were applied to the glass/steel substrates by using a film applicator coater (Bird type applicator with a constant slot width, product of Zehntner GmbH, Schwerzenbach, Switzerland). The slot width was 150 µm for application on the glass panels and 250 µm for application on the steel panels. The paint films on the panels were allowed to dry for 10 days (except for the panels intended for flash corrosion examination) in an air-conditioned room.

For determination of true nanoparticle content in the LM latex film, the latexes (both LM and L0) were cast into silicone molds to obtain loose films, which were then allowed to dry to a constant weight prior to ICP–OES (inductively coupled plasma–optical emission spectroscopy) measurement. For the antimicrobial efficiency tests, the latexes were applied to sterile filter paper (Munktell Filtrak 391, 15 cm in diameter, grammage 84 g/m^2) squares with a size of 5 cm × 5 cm. The paint was applied to the filter paper with a brush in perpendicular directions in 4 layers, with a minimum drying time of 4 h between the layers; the tests themselves were performed after a drying period of 10 days.

Each test was performed in triplicate. All of the paint films—on glass, steel and filter paper and in silicone molds—were exposed to a temperature of 21 ± 2 °C and relative humidity of 55% in an air-conditioned room according to ČSN EN 23270 prior to the tests.

2.7. Paint Film Property Assessments

The true magnesium nanoparticle contents of the paint films were determined by ICP–OES (inductively coupled plasma–optical emission spectroscopy) on a Thermo Scientific iCAP 7000 Series instrument (Thermo Fisher Scientific, Waltham, MA, USA) [50]. The paint film structure at a fracture plane was measured by scanning electron microscopy (SEM) on a LYRA 3 instrument (Tescan, Brno, Czech Republic).

The physical properties of the paint films were evaluated according to ČSN EN ISO 1522—Paints and varnishes—Pendulum damping test; Persoz type pendulum (3034M001 pendulum, Elcometer Instruments GmbH, Aalen, Germany).

The mechanical properties (mechanical resistance) of the paint films were assessed according to ČSN EN ISO 6272-2—Paints and varnishes—Rapid-deformation (impact resistance) tests, viz. through measurements on an Elcometer 1615 variable impact tester (Elcometer Instruments GmbH, Aalen, Germany). Tests according to ČSN ISO 2409, such as the cross-cut test, were also made. An Elcometer cross-cut system (Elcometer Instruments GmbH, Aalen, Germany) with 6 parallel knives 1 mm apart was used.

Chemical resistance of the paint films was assessed according to ASTM D-4752-10—rubbing test with methyl ethyl ketone (MEK).

Flash corrosion resistance of the paint films was assessed through a laboratory test to identify/measure any flash corrosion [41]. The tests were made on paint films deposited on steel panels which, after drying at 21 ± 2 °C, RH 50 ± 5% for 2 h, were stored in a refrigerator at 5 °C for 16 h. After removal from the refrigerator, the entire paint film was uniformly covered with a filter paper that was pre-wetted with distilled water, and the system was covered with a heavy glass plate to achieve full contact between the paint film and water. The water was allowed to act for 2 h at room temperature. The filter paper was then removed, the paint film was dried, and corrosion phenomena were scored as per ASTM D 610-85; coloration was scored using Gardner's iodometric scale (Table 3) [51].

Table 3. Gardner's iodometric scale.

Degree	**1**	**2**	**3**	**4**	**5**	**6**	**7**	**8**	**9**	**10**	**11**	**12**	**13**	**14**
mg I_2/100 cm^3	1	2	4	6	10	20	30	45	65	100	150	200	300	500

The antimicrobial efficiency of the paint films was assessed with respect to the collection of the strains *Staphylococcus aureus* CCM 2022, *Escherichia coli* CCM 3954 and *Pseudomonas aeruginosa* CCM 3955 and to the molds *Penicillium chrysogenum* CCM 8034 and *Aspergillus brasiliensis* CCM 8222 (Czech Collection of Microorganisms, Masaryk University, Brno, Czech Republic). Twenty-four-hour bacteria cultures and 5-day mold cultures were used for the testing. The microbial cultures were suspended in saline at concentrations of approximately 10^6 CFU/mL (bacteria) and 10^6 spores/mL (molds). A sterile sample of the smear was applied to the center of a Petri dish with agar, followed by 0.1 mL of the microbial suspension. The suspension was spread uniformly over the entire surface with an L-shaped hockey stick and the bacterial samples inoculated in this way were incubated at 37 °C for 24 h; the molds were incubated at 25 °C for 7 days. The microorganism density was evaluated by inoculating the suspension onto pure agar, which was expected to contain 300 bacterial colonies and 100% agar covering with the mold after the process. The mold increase on the material tested was evaluated after incubation. Where the bactericidal efficiency was examined, the sample was imprinted onto agar and incubation was conducted at 37 °C for 24 h. The percent bacterial colony increase was measured after the incubation procedure.

Each test was performed in triplicate and the final result was represented by the arithmetic mean of the 3 observed values.

3. Results and Discussion

3.1. Properties of the Latexes

The coagulate content, zeta-potential, particle size, pH, apparent viscosity and MFFT were measured for the two latex types (Table 4). Based on the coagulate content of the LM binder relative to the L0 binder, the presence of the nanostructural MgO brought about a slight reduction in the colloidal stability of the dispersion during the synthesis. This effect was presumably due to the increase in ionic

strength of the dispersion environment caused by the dissolution of a significant fraction of the MgO (MgO solubility in water at 30 °C is 86 mg/L).

The Zeta-potential was also lower in the LM binder than in the L0 binder, but both values were above ±30 mV, so both latexes could be considered adequately stable.

Particle size was measured in order to determine whether the agglomerates (in which form the MgO nanoparticles had been added to the latex) disintegrated during the synthesis and whether they were actually present in the form of nanoparticles. The dispersion contained no significant quantities of agglomerates of the nanoparticles or of coagulated latex particles. The pH of the latex L0 was 2.1 prior to alkalinization, mainly due to the sulfate groups emerging from the reaction between the initiator and water. The presence of sulfate and carboxyl groups on the surface of the latex particles, due to the adsorbed molecules of the emulsifier and the copolymerized methacrylic acid, could have also contributed to this. The pH of the LM latex was 10.34, apparently due to the hydration of the MgO nanoparticles, giving rise to insoluble nanoparticles, mainly of $Mg(OH)_2$, or to MgO nanoparticles covered with a layer of $Mg(OH)_2$ and to dissociated Mg^{2+} and OH^- ions, the latter causing the increase in the latex pH.

Apparent viscosity was found to increase (from 10.8 to 30.97 mPa·s) in the L0 binder after alkalinization due to the effect referred to as the alkali-swelling of latex particles [52]. Appreciably increased viscosity (90.86 mPa·s) was also found for the LM binder, once again due to the increased pH inducing alkali-swelling of the latex particles.

The MFFT data provided evidence that the two latexes formed paint films at room temperature, where the MFFT of the LM latex did not exceed 2 °C. These results are in good agreement with detected T_g values of 15.4 °C and 5.0 °C for the L0 polymer and the LM polymer, respectively. The differences in the behavior of the two binder types LM and L0 may have been due to the increased hydroplasticization of the emulsion copolymers containing carboxylic groups. It is known that the neutralized (dissociated) carboxylic groups impart an increased content of molecularly bonded (hydroplasticizing) water in emulsion copolymers [53,54]. Presumably, the dissolution of a fraction of MgO in water, giving rise to dissociated hydroxyl and magnesium ions, induced the conversion of the non-dissociated carboxylic groups (−COOH) to dissociated carboxylate groups ($-COO^-$), which are capable of bonding appreciable amounts of water by molecular mechanisms.

Table 4. Basic properties of evaluated binders.

Sample	Coagulate Content (%)	Zeta-Potential (mV)	Particle Size $d_{50}/d_{10}/d_{90}$ (nm)	pH (–)	Apparent Viscosity (mPa/s)	MFFT (°C)
LM	2.99 ± 0.53	−30.9 ± 0.6	179.8 ± 2.81/177.5 ± 1.98/ 181.6 ± 2.32	10.34 ± 0.11	90.86 ± 3.96	1.9 ± 0.2
L0	0.1 ± 0.08	−39.0 ± 1.7	140.3 ± 2.54/139.1 ± 2.95/ 141.8 ± 3.03	8.44 ± 0.03	30.97 ± 2.43	5.8 ± 0.4

In-Can Preservation testing of the aqueous dispersions provided evidence of the antimicrobial efficiency of the acrylate binder containing magnesium nanoparticles. While the reference latex with no nanoparticles exhibited the presence of bacteria at a density of 1×10^6 CFU/mL and a high coverage by yeasts, the LM latex exhibited no microorganisms (Figure 1). This effect can be ascribed to the peroxidation of lipids and the formation of reactive oxygen species, alkalinity latex and/or the presence of sharp-edged magnesium nanoparticles. It should be mentioned here, however, that the In-Can test provides only quantitative information. The nature of present microbial species was not therefore detected.

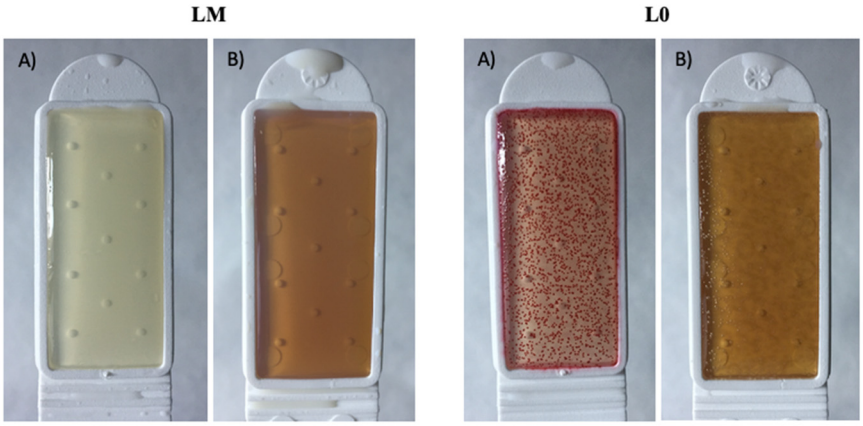

Figure 1. Results of In-Can Stability Testing of Aqueous Polymer Dispersions: (**A**) Bacteria, (**B**) Mold and/or Yeast.

3.2. Properties of the Paint Films

The true magnesium nanoparticle content in the dry paint film was determined by ICP–OES and served to calculate the magnesium nanoparticle content of the binder (Table 5). The true nanoparticle content of the film (1.11%) was found to be lower than the theoretical content based on the amount that was initially added to the reaction mixture (1.5% with respect to the total monomer content), in all probability due to the increased formation of the magnesium nanoparticle-rich coagulate (12.08 g) during the synthesis.

Table 5. Determination of nanoparticles content in coating film and aqueous dispersion by ICP–OES.

Sample	Theoretical Nanoparticle Content in Film (%)	Content Mg (mg/kg)	Actual Nanoparticle Content in Film (%) *	Actual Nanoparticle Content in Dispersion (%)
LM	1.5	6680 ± 29	$1.108 \pm 4.8 \times 10^{-3}$	$0.443 \pm 1.8 \times 10^{-3}$
L0	0	0.713	-	-

* Percentage of magnesium nanoparticles in a dried coating film was calculated using the formula: The actual nanoparticle content in film (%) = (Sum Mg (mg/kg) × M_r(MgO) × 10^{-4})/M_r(Mg). The calculation was based on the simplified assumption that all the determined Mg in the coating film was only in the form of MgO.

The presence and distribution of the magnesium nanoparticles in the coating's films were examined by SEM. The photographs of the LM coating film shown in Figure 2 were obtained in the secondary and backscattered electron modes: the former Figure 2a primarily describes the sample topography, whereas the latter Figure 2b manifests the elemental contrast (i.e., the material composition of the sample). Although the magnesium nanoparticles were not distinguished clearly in the polymer matrix, evidence was gained to show that the film contained uniformly distributed isolated spherical nanoparticles whose size was in the order of tens of nanometers (which is a prerequisite for the paint film transparency) and that the nanostructural MgO agglomerates had been disintegrated. The poor detectability of the nanoparticles can suggest their partial dissolution in latex aqueous medium, as MgO exhibits a slight solubility in water (the solubility data were mentioned above).

The comparison of the coating films obtained by using the two latex types, demonstrated the effect of the magnesium nanoparticles (Table 6). The LM latex exhibited higher resistance to mechanical damage (resistance to the drop in weight and the adhesion test) and a lower surface hardness (by 4.2%). These effects are in all probability due to hydroplasticization of the emulsion copolymers, as mentioned above. The resistance to MEK is substantially (by 90.7%) better for the LM binder than for the L0 binder, presumably owing to the higher network density due to the formation of ionic bonds between the magnesium cations (Mg^{2+}) and the carboxylic groups on the polymeric chains.

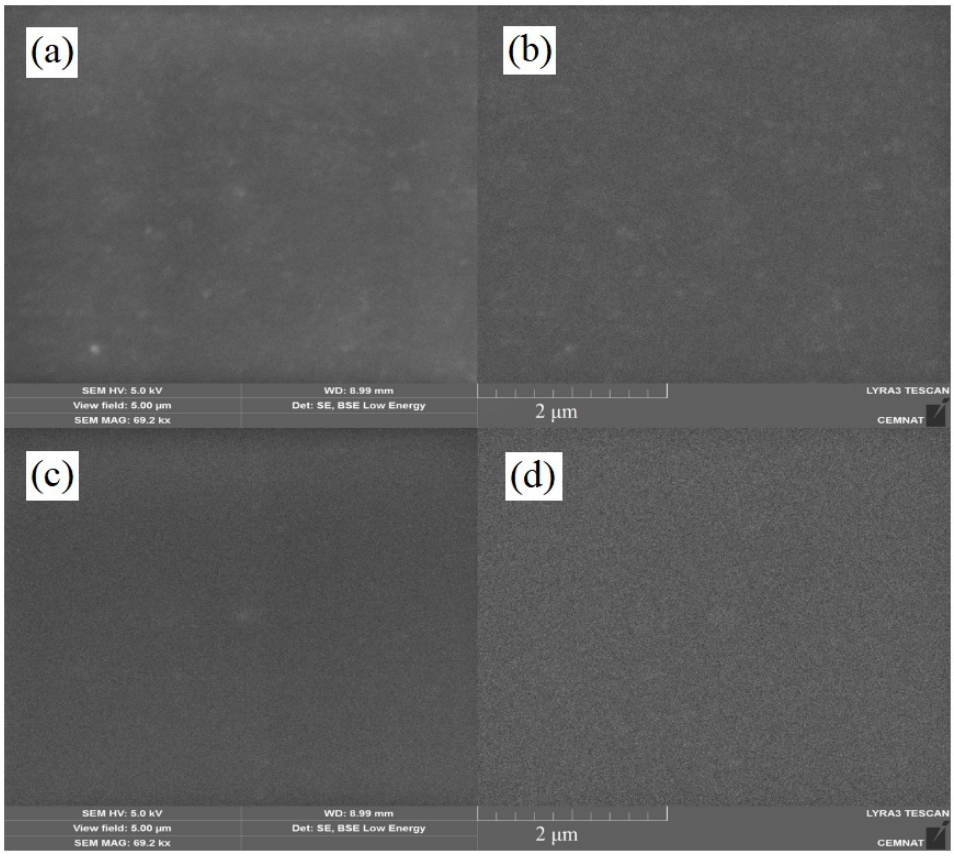

Figure 2. The SEM images of the surface of the cryo-fractured coating film sample LM (**a**,**b**) and L0 (**c**,**d**) taken in secondary (**a**,**c**) and backscattered electrons (**b**,**d**).

Table 6. Evaluation of coating films of self-crosslinking latexes (DFT = 50 ± 10 µm).

Sample	Surface Hardness (%)	Mechanical Damage		MEK (s)	Flash Corrosion	
		Rapid-Deformation (cm)	Cross-Cut Test (st.)		ASTM (%)	Scale (st.)
LM	22.8 ± 0.2	>100	0	>300	0.01	1
L0	27.0 ± 0.2	85 ± 2	1	28 ± 3	3	8

Flash corrosion of the steel substrate was only observed beneath the L0 latex (Figure 3). It can, therefore, be concluded that the MgO nanoparticles make up an efficient flash corrosion inhibitor, probably based on the alkaline action that caused the pH close to the steel to shift to a range where the steel substrate corrosion is suppressed [55].

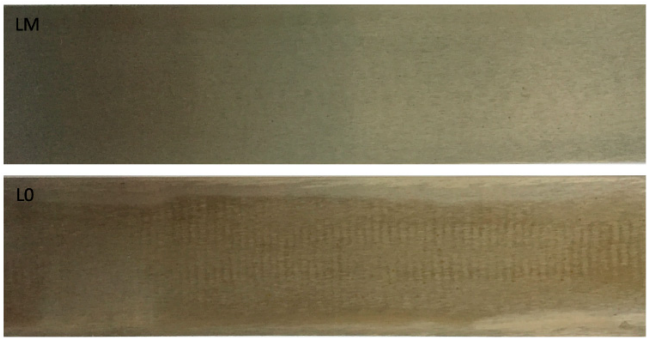

Figure 3. Signs of flash corrosion after an accelerated laboratory test of non-pigmented coating films.

3.3. Antimicrobial Efficiency of the Paint Films

Firstly, the antimicrobial efficiency of the non-pigmented coating films was examined according to the extent of bacteria growth on the coating sample surface (Table 7). The testing revealed that the LM coatings exhibited the maximum antibacterial effect (no bacteria growth) against *S. Aureus* and *E. coli*, the antibacterial effect of 90 ± 5% (10 ± 5% of coating surface was grown by bacteria) against *P. aeruginosa* and a moderate antifungal effect. In contrast, the L0 coatings showed no significant antimicrobial effect against all the tested bacterial and fungal strains. To distinguish between the bactericidal and bacteriostatic activity of the LM coatings, tests on imprints were further performed (Table 8). The testing revealed the bacteriostatic activity of LM coatings, which means that the bacteria were not killed, but stopped from reproducing at the interface of the coatings.

Table 7. Antimicrobial efficiency of non-pigmented coating films.

Sample	Antimicrobial Effect (%)				
	S. Aureus	***E. Coli***	***P. Aeruginosa***	***P. Chrysogenum***	***A. Crasiliensis***
LM	100	100	90 ± 5	50 ± 10	50 ± 10
L0	0	0	0	0	0

Table 8. Antimicrobial efficiency of non-pigment coating films (test on imprints).

Sample	Antimicrobial Effect (%)		
	S. Aureus	***E. Coli***	***P. Aeruginosa***
LM	70 ± 10	60 ± 10	50 ± 5
L0	0	0	0

The antimicrobial action mechanism of the MgO nanoparticles has not yet been fully elucidated. Peroxidation of lipids and the formation of reactive oxygen species, which may prevent the growth of microorganisms, have been demonstrated (Figure 4) but are insufficient for a microbicidal effect to appear at the existing MgO nanoparticle concentration. The alkalinity of latex, due to the presence of hydroxyl ions emerging from the hydration of MgO nanoparticles as described in detail above, may also contribute to the suppression of microorganism growth. The antimicrobial efficiency of the magnesium nanoparticles against all the tested bacterial and fungal strains are outlined in Figure 5.

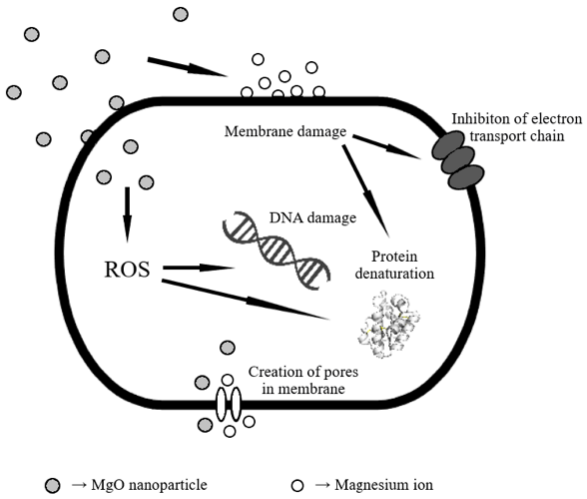

Figure 4. The antimicrobial action mechanism of MgO nanoparticles.

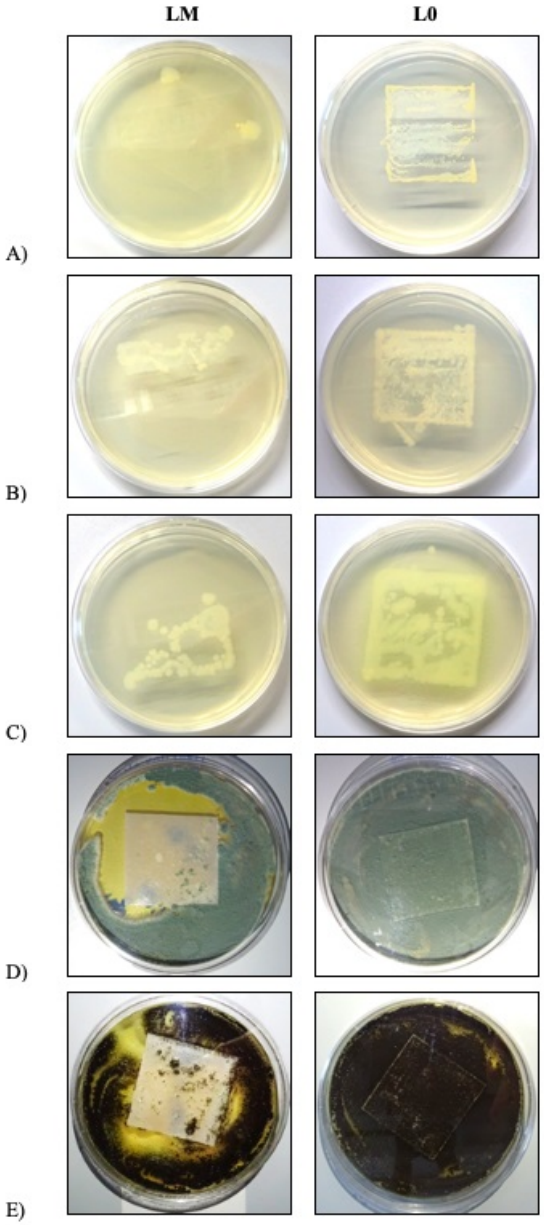

Figure 5. Visualization of antimicrobial activity of non-pigmented coating films against: (**A**) *S. aureus*, (**B**) *E. coli*, (**C**) *P. aeruginosa*, (**D**) *P. chrysogenum*, (**E**) *A. brasiliensis*.

The antimicrobial efficiency of the pigmented paint films was also examined by adding 2% and 10% (*w*/*w*) of selected pigments and fillers to both the LM latex and the reference L0 latex (blank); as mentioned earlier, the blank exhibits no antimicrobial efficiency at all (Tables 7 and 8). The results are presented in Tables 9 and 10. The data show that the amount (*w*/*w*) of a pigment or filler added only slightly affects the antimicrobial efficiency of the system. The best results in this respect were attained with Zn- and Mg-based compounds and TiO_2. In particular, the increased antimicrobial effect of LM coatings films was determined against *S. aureus* for five additives out of 10 used (Nano–MgO, Nano–ZnO, ZnO, TiO_2 and $MgCO_3$), against *E. coli* for three additives out of 10 used (Nano–MgO, ZnO and $MgCO_3$), against *P. aeruginosa* for two additives out of 10 used (Nano–MgO and $MgCO_3$), against *P. chrysogenum* for one additives out of 10 used (ZnO) and against *A. Brasiliensis* for three additives out of 10 used (Nano–MgO, Nano–ZnO and ZnO). It is also apparent from the measurement that in the case of the reference L0 latex, only the Nano–MgO additive has a significant antimicrobial effect.

Table 9. Antimicrobial effect of LM coating films.

LM + Pigment	*w/w* %	Antimicrobial Effect (%)				
		S. Aureus	*E. Coli*	*P. Aeruginosa*	*P. Chrysogenum*	*A. Brasiliensis*
Nano–MgO	2	100	95 ± 2.9	90 ± 2.9	50 ± 10	100
	10	100	100	100	50 ± 7.6	100
Nano–ZnO	2	100	50 ± 2.9	30 ± 5	40 ± 2.9	100
	10	100	60 ± 7.6	40 ± 2.9	40 ± 5	100
ZnO	2	100	95 ± 2.9	40 ± 7.6	60 ± 7.6	100
	10	100	95 ± 2.9	40 ± 2.9	60 ± 10	100
TiO_2	2	90 ± 2.9	60 ± 5	40 ± 5	10 ± 10	0
	10	90 ± 2.9	40 ± 10	20 ± 10	10 ± 10	0
$MgCO_3$	2	100	80 ± 2.9	70 ± 2.9	50 ± 10	50 ± 15
	10	100	90 ± 5	70 ± 7.6	50 ± 10	50 ± 10
$BaSO_4$	2	75 ± 2.9	60 ± 5	40 ± 7.6	0	0
	10	40 ± 7.6	60 ± 5	20 ± 5	0	0
ZnS	2	50 ± 5	45 ± 2.9	30 ± 5	0	0
	10	50 ± 2.9	40 ± 2.9	35 ± 2.9	0	0
ZnS + $BaSO_4$	2	50 ± 2.9	40 ± 2.9	20 ± 2.9	0	0
	10	50 ± 2.9	40 ± 2.9	20 ± 5	0	0
Muskovit	2	20 ± 5	15 ± 7.6	10 ± 2.9	0	0
	10	30 ± 2.9	20 ± 5	10 ± 2.9	0	0
$CaCO_3$	2	20 ± 5	15 ± 2.9	0	0	0
	10	20 ± 2.9	15 ± 2.9	0	0	0

Table 10. Antimicrobial effect of L0 coating films.

L0 + Pigment	*w/w* %	Antimicrobial Effect (%)				
		S. Aureus	*E. Coli*	*P. Aeruginosa*	*P. Chrysogenum*	*A. Brasiliensis*
Nano–MgO	2	55 ± 2.9	50 ± 2.9	25 ± 2.9	0	0
	10	60 ± 5	70 ± 5	30 ± 2.9	0	0
Nano–ZnO	2	20 ± 5	15 ± 2.9	15 ± 2.9	0	0
	10	20 ± 10	15 ± 2.9	25 ± 5	0	0
ZnO	2	15 ± 2.9	10 ± 2.9	5 ± 2.9	0	0
	10	15 ± 2.9	0	5 ± 2.9	0	0
TiO_2	2	20 ± 2.9	25 ± 2.9	10 ± 5	0	0
	10	35 ± 5	20 ± 7.6	10 ± 2.9	0	0
$MgCO_3$	2	15 ± 2.9	10 ± 2.9	10 ± 2.9	0	0
	10	10 ± 2.9	20 ± 5	10 ± 2.9	0	0
$BaSO_4$	2	0	5 ± 2.9	0	0	0
	10	5 ± 2.9	0	0	0	0
ZnS	2	20 ± 2.9	20 ± 5	5 ± 2.9	0	0
	10	20 ± 2.9	35 ± 7.6	10 ± 2.9	0	0
ZnS + $BaSO_4$	2	0	0	0	0	0
	10	5 ± 2.9	0	0	0	0
Muskovit	2	0	10 ± 2.9	10 ± 5	0	0
	10	10 ± 2.9	10 ± 2.9	0	0	0
$CaCO_3$	2	0	0	0	0	0
	10	0	5 ± 2.9	0	0	0

The MgO nanoparticles are the same as during the synthesis of the LM latex. The addition of only 2% (*w*/*w*) to attain a total true concentration of 3.11% MgO nanoparticles provided evidence that the efficiency of the MgO nanoparticles improves with their increasing concentration, and a true concentration of 11.11% gives rise to microbicidal effects. The mechanism of action of

ZnO nanoparticles is the same as with the MgO nanoparticles and, moreover, is enhanced by the photooxidative effect [28,56,57]. The efficiency of TiO_2 has been ascribed to its photocatalytic activity [58]. The remaining pigments and fillers exhibited a minimal antimicrobial effect only, and even counteracted the antimicrobial efficiency of the LM latex by shielding the magnesium nanoparticles in some cases.

The potential savings of the antimicrobial additive zinc pyrithione were examined within the range recommended for coatings [56,59] and below, i.e., at 0.1% to 0.3%. Table 11 indicates that the amount of additives in the LM latex (in contrast to L0) can be reduced by one-third or more without losing the microbicidal efficiency against the bacterial cultures tested. As little as 0.1% and 0.3% zinc pyrithione is sufficient to prevent fungal and bacterial growth, respectively. The mechanism of action of this additive is not precisely known, but its antifungal effect is assumed to be related to its ability to block the proton pump, which energizes the transport mechanism [60,61].

Table 11. Antimicrobial effect of coating films containing zinc pyrithione (ZP).

Binder	ZP *w/w* (%)	Antimicrobial Effect (%)				
		S. Aureus	***E. Coli***	***P. Aeruginosa***	***P. Chrysogenum***	***A. Brasiliensis***
LM	0.3	100	100	100	100	100
	0.2	100	100	100	100	100
	0.1	100	100	90 ± 5	100	100
L0	0.3	100	100	100	100	100
	0.2	70 ± 5	70 ± 2.9	30 ± 2.9	100	100
	0.1	70 ± 7.6	50 ± 5	20 ± 5	100	100

The observed data provide evidence that the magnesium nanoparticles possess certain antimicrobial properties and their combination with the antimicrobial additive zinc pyrithione exhibit a synergistic effect.

4. Conclusions

Environmentally friendly binders, based on water-dilutable self-crosslinking acrylate dispersions containing MgO nanoparticles, were studied. The binder that contained about 0.4% (*w/w*) magnesium oxide nanoparticles exhibited colloidal stability as well as In-Can preservation and provided, as expected, paints whose films exhibited a high mechanical resistance, chemical resistance and antimicrobial properties. The system thereby displays promise for use in antimicrobial coatings where the microbicidal effect is required. Furthermore, evidence was obtained demonstrating that a microbicidal effect against all of the cultures tested can be obtained with systems in which the amounts of antimicrobial additives are reduced by one-third or more compared to systems in which no MgO nanoparticles are present. The high mechanical resistance, chemical resistance and resistance against flash corrosion make the system a universal coating material.

Author Contributions: Conceptualization, D.S., A.K. and J.M.; methodology, D.S., A.K., J.M. and M.P.; software, D.S.; validation, D.S., A.K. and J.M.; formal analysis, D.S.; investigation, D.S. and J.M.; resources, D.S.; data curation, D.S.; writing—original draft preparation, D.S.; writing—review and editing, D.S., A.K., J.M. and M.P.; visualization, D.S.; supervision, A.K. All authors have read and agreed to the published version of the manuscript.

Funding: This research received no external funding.

Conflicts of Interest: The authors declare no conflicts of interest.

References

1. Bouchaala, A. Volatile Organic Compounds removal methods: A review. *Am. J. Biochem. Biotechnol.* **2012**, *8*, 220–229. [CrossRef]
2. Chang, J.C.S.; Fortmann, R.; Roache, N.; Lao, H.-C. Evaluation of Low-VOC Latex Paints. *Indoor Air* **1999**, *9*, 253–258. [CrossRef] [PubMed]

3. Nikiema, J.; Dastous, P.-A.; Heitz, M. Elimination of Volatile Organic Compounds by Biofiltration: A Review. *Rev. Environ. Health Dow Coat. Mater.* **2007**, *22*, 273–294. [CrossRef]
4. Swartz, N.A.; Wood, K.A.; Lasseter Clare, T. Characterizing and improving performance properties of thin solid films produced by weatherable water-borne colloidal suspensions on bronze substrates. *Prog. Org. Coat.* **2012**, *75*, 215–223. [CrossRef]
5. Athawale, V.D.; Nimbalkar, R.V. Waterborne Coatings Based on Renewable Oil Resources: An Overview. *J. Am. Oil Chem. Soc.* **2011**, *88*, 159–185. [CrossRef]
6. Joseph, R. Low-VOC Waterborne Coatings. *Met. Finish.* **1999**, *97*, 127–134. [CrossRef]
7. Kurowski, G.; Vogt, O.; Ogonowski, J. Paint-degrading microorganisms. *Czasopismo Techniczne* **2017**, *114*, 81–92.
8. Peleg, A.Y.; Hooper, D.C. Hospital-acquired infections due to gram-negative bacteria. *N. Engl. J. Med.* **2010**, *362*, 1804–1813. [CrossRef]
9. Rosenthal, V.D.; Maki, D.G.; Salomao, R.; Moreno, C.A.; Mehta, Y.; Higuera, F.; Cuellar, L.E.; Arikan, O.A.; Abouqal, R.; Leblebicioglu, H. Device-associated nosocomial infections in 55 intensive care units of developing countries. *Ann. Int. Med.* **2006**, *145*, 582–591. [CrossRef]
10. Válka, R.; Machotová, J.; Podzimek, Š. Development of the molecularweight of styrene-acrylate and methylmethacrylate-acrylate emulsion copolymers. *Chemagazín* **2017**, *10*, 105–111.
11. Parvate, S.; Mahanwar, P. Advances in self-crosslinking of acrylic emulsion: What we know and what we would like to know. *J. Dispers. Sci. Technol.* **2019**, *40*, 519–536. [CrossRef]
12. Liu, Y.; Hou, C.; Jiao, T.; Song, J.; Zhang, X.; Xing, R.; Zhou, J.; Zhang, L.; Peng, Q. Self-Assembled AgNP-Containing Nanocomposites Constructed by Electrospinning as Efficient Dye Photocatalyst Materials for Wastewater Treatment. *Nanomaterials* **2018**, *8*, 35. [CrossRef] [PubMed]
13. Machotová, J.; Rückerová, A.; Kalendová, A.; Pejchalová, M. Waterborne self-crosslinking polymer dispersions with biocidal effect. *Chemagazín* **2017**, *10*, 89–95.
14. Wang, R.; Wang, J.-F.; Wang, X.-W.; He, Y.-F.; Zhu, Y.-F.; Jiang, M.-L. Preparation of acrylate-based copolymer emulsion and its humidity controlling mechanism in interior wall coatings. *Prog. Org. Coat.* **2011**, *71*, 369–375. [CrossRef]
15. Fonkwo, P.N. Pricing infectious disease: The economic and health implications of infectious diseases. *EMBO Rep.* **2008**, *9*, 13–17. [CrossRef]
16. Kurzbaum, E.; Iliasafov, L.; Kolik, L.; Starosvetsky, J.; Bilanovic, D.; Butnarium, M.; Armon, R. From the Titanic and other shipwrecks to biofilm prevention: The interesting role of polyphenol-protein complexes in biofilm inhibition. *Sci. Total Environ.* **2019**, *658*, 1098–1105. [CrossRef]
17. Glinel, K.; Thebault, P.; Humblot, V.; Pradier, C.M.; Jouenne, T. Antibacterial surfaces developed from bio-inspired approaches. *Acta Biomater.* **2012**, *8*, 1670–1684. [CrossRef]
18. Thokala, N.; Kealey, C.; Kennedy, J.; Brady, D.B.; Farrell, J. Comparative activity of silver-based antimicrobial composites for urinary catheters. *Int. J. Antimicrob. Agents* **2018**, *52*, 166–171. [CrossRef]
19. Gómez de Saravia, S.G.; Rastelli, S.E.; Blustein, G.; Viera, M.R. Natural compounds as potential algaecides for waterborne paints. *J. Coat. Technol. Res.* **2018**, *15*, 1191–1200. [CrossRef]
20. Kuznetsov, D.N.; Kobrakov, K.I.; Ruchkina, A.G.; Stankevich, G.S. Biologically active synthetic organic dyes. *Izvestiya Vysshikh Uchebnykh Zavedeniy Khimiya Khimicheskaya Tekhnologiya* **2017**, *60*, 4–33. [CrossRef]
21. Ventola, C.L. The Antibiotic Resistance Crisis: Part 1: Causes and Threats. *P T Peer Rev. J. Formul. Manag.* **2015**, *40*, 277–283.
22. Spellberg, B.; Bartlett, J.G.; Gilbert, D.N. The Future of Antibiotics and Resistance. *N. Engl. J. Med.* **2013**, *368*, 299–302. [CrossRef] [PubMed]
23. Fair, R.J.; Tor, Y. Antibiotics and Bacterial Resistance in the 21st Century. *Perspect. Med. Chem.* **2014**, *6*, 25–64. [CrossRef] [PubMed]
24. Kandelbauer, A.; Widsten, P. Antibacterial melamine resin surfaces for wood-based furniture and flooring. *Prog. Org. Coat.* **2009**, *65*, 305–313. [CrossRef]
25. Fymat, A.L. Antibiotics and Antibiotic Resistance. *Biomed. J. Sci. Tech. Res.* **2017**, *1*, 1–16. [CrossRef]
26. Azam, A.; Ahmed, A.S.; Oves, M.; Khan, M.S.; Habib, S.S.; Menic, A. Antimicrobial activity of metal oxide nanoparticles against Gram-positive and Gram-negative bacteria: A comparative study. *Int. J. Nanomed.* **2012**, *7*, 6003–6009. [CrossRef]

27. Dizaj, S.M.; Lotfipour, F.; Barzegar-Jalali, M.; Zarrintan, M.H.; Adibkia, K. Antimicrobial activity of the metals and metal oxide nanoparticles. *Mater. Sci. Eng. C* **2014**, *44*, 278–284. [CrossRef]
28. Bonnefond, A.; González, E.; Asua, J.M.; Leiza, J.R.; Kiwi, J.; Pulgarin, C.; Rtimi, S. New evidence for hybrid acrylic/TiO_2 films inducing bacterial inactivation under low intensity simulated sunlight. *Colloids Surf. B Biointerfaces* **2015**, *135*, 1–7. [CrossRef]
29. Yan, W.; Zhang, X.; Zhu, Y.; Chen, H. Synthesis and characterization of self-crosslinkable zinc polyacrylate lattices at room temperature. *Iran. Polym. J.* **2012**, *21*, 631–639. [CrossRef]
30. Yang, L.; Xie, Z.; Li, Z. Studies on Acrylate Copolymer Soap-Free Waterborne Coatings Crosslinked by Metal Ions. *J. Appl. Polym. Sci.* **1997**, *66*, 2457–2463. [CrossRef]
31. Balard, H.; Papirer, E. Characterization and modification of fillers for paints and coatings. *Prog. Org. Coat.* **1993**, *22*, 1–17. [CrossRef]
32. Mirtalebi, S.S.; Almasi, H.; Alizadeh Khaledabad, M. Physical, morphological, antimicrobial and release properties of novel MgO-bacterial cellulose nanohybrids prepared by in-situ and ex-situ methods. *Int. J. Biol. Macromol.* **2019**, *128*, 848–857. [CrossRef] [PubMed]
33. Karakas, F.; Pyrgiotakis, G.; Celik, M.S.; Moudgil, B.M. Na-Bentonite and MgO Mixture as a Thickening Agent for Water-Based Paints. *KONA Powder Part J.* **2011**, *29*, 96–106. [CrossRef]
34. Walling, S.A.; Provis, J.L. Magnesia-Based Cements: A Journal of 150 Years, and Cements for the Future? *Chem. Rev.* **2016**, *116*, 4170–4204. [CrossRef] [PubMed]
35. Ge, S.; Wang, G.; Shen, Y. Cytotoxic effects of MgO nanoparticle on human umbilical vein of endothelia cells In Vitro. *IET Nanobiotechnol.* **2011**, *5*, 36–40. [CrossRef] [PubMed]
36. Ishigaki, H.; Buckley, D.H. *Effects of Environment on Microhardness of Magnesium Oxide*; NASA Technical Paper 2002; NASA Lewis Research Center: Cleveland, OH, USA, 1982.
37. Dhermendra, K.T.; Behari, J. Application of Nanoparticles in waste water treatment. *World Appl. Sci. J.* **2008**, *3*, 417–433.
38. Nguyen, N.-Y.T.; Grelling, N.; Wetteland, C.L.; Rosario, R.; Liu, H. Antimicrobial Activities and Mechanisms of Magnesium Oxide Nanoparticles (nMgO) against Pathogenic Bacteria, Yeasts, and Biofilms. *Sci. Rep.* **2018**, *8*, 1–23. [CrossRef]
39. EL-Mekkawi, D.M.; Selim, M.M.; Hamdi, N.; Hassan, S.A.; Ezzat, A. Studies on the influence of the physicochemical characteristics of nanostructured copper, zinc and magnesium oxides on their antibacterial activities. *J. Environ. Chem. Eng.* **2018**, *6*, 5608–5615. [CrossRef]
40. Tang, Z.-X.; Lv, B.-F. MgO nanoparticles as antibacterial agent: Preparation and activity. *Braz. J. Chem. Eng.* **2014**, *31*, 591–601. [CrossRef]
41. Novák, P. Druhy koroze kovů. *Koroze A Ochrana Materiálu* **2005**, *49*, 75–82.
42. Šňupárek, J. *Makromolekulární Chemie: Úvod Do Chemie A Technologie Polymer*, 3rd ed.; Univerzita Pardubice: Pardubice, Czech Republic, 2014; pp. 37–123.
43. Kalendová, A. *Metody Testování Vlastností Organických Povlaků: Díl 1, Korozně-Inhibiční Účinnost Organických Povlaků*, 1st ed.; Univerzita Pardubice: Pardubice, Czech Republic, 2001; pp. 42–141.
44. Kalendová, A. *Antikorozní Pigmenty A Nátěrové Hmoty: Sborník Příspěvků Odborné Conference*, 1st ed.; Univerzita Pardubice: Pardubice, Czech Republic, 2002; pp. 110–111.
45. Fox, T.G.; Flory, P.J. 2nd-Order transition temperatures and related properties of polystyrene. 1. Influence of molecular weight. *J. Appl. Phys.* **1950**, *21*, 581–591. [CrossRef]
46. Bhattacharjee, S. DLS and zeta potential–What they are and what they are not? *J. Control. Release* **2016**, *235*, 37–351. [CrossRef] [PubMed]
47. Dvořák, J.; Číhalík, J.; Suk, V. *Příručka měření pH*, 1st ed.; SNTL: Praha, Czech Republic, 1975; pp. 38–167.
48. Diesel Fuel Test Kit. Available online: https://www.dieselfueltestkit.com/ft-bug-test-kit-for-diesel-bacteria-testing/?fbclid=IwAR0ASDDOfCHmNW3i2IvPRehl0oK7ORC7M80fE_Hc3t2voVMGupCC91V2BHM (accessed on 31 March 2020).
49. Kalendová, A. *Technologie Nátěrových Hmot II: Povrchové Úpravy A Způsoby Předúpravy Materiálů*, 1st ed.; Univerzita Pardubice: Pardubice, Czech Republic, 2003; pp. 51–128.
50. Moore, G.L. *Introduction to Inductively Coupled Plasma Atomic Emission Spectrometry*, 1st ed.; Elsevier Science: Randburg, South Africa, 1988; pp. 1–309.
51. Kalendová, A. Methods for testing and evaluating the flash corrosion. *Prog. Org. Coat.* **2002**, *44*, 201–209. [CrossRef]

52. Šňupárek, J.; Quadrat, O.; Horský, J. Effect of styrene and methyl methacrylate comonomers in ethyl acrylate/methacrylic acid latex on particle alkali-swellability, film formation and thickening with associative thickeners. *Prog. Org. Coat.* **2005**, *54*, 99–103. [CrossRef]
53. Tsavalas, J.G.; Sundberg, D.C. Hydroplasticization of Polymers: Model Predictions and Application to Emulsion Polymers. *Langmuir* **2010**, *26*, 6960–6966. [CrossRef] [PubMed]
54. Jiang, B.; Tsavalas, J.G.; Sundberg, D.C. Water whitening of polymer films: Mechanistic studies and comparison between water and solvent borne films. *Prog. Org. Coat.* **2017**, *105*, 56–66. [CrossRef]
55. Kalenda, P.; Veselý, D.; Antoš, P. *Koroze A Protikorozní Ochrana Kovových Materiálů*, 1st ed.; Univerzita Pardubice: Pardubice, Czech Republic, 2003.
56. Samu, G.F.; Veres, Á.; Tallósy, S.P.; Janovák, L.; Dékány, I.; Yepez, A.; Luque, R.; Janáky, C. Photocatalytic, photoelectrochemical, and antibacterial activity of benign-by-design mechanochemically synthesized metal oxide nanomaterials. *Catal. Today* **2017**, *284*, 3–10. [CrossRef]
57. Bonnefond, A.; González, E.; Asua, J.M.; Leiza, J.R.; Ieva, E.; Brinati, G.; Carella, S.; Marrani, A.; Veneroni, A.; Kiwi, J.; et al. Stable Photocatalytic Paints Prepared from Hibrid Core-Shell Fluorinated/Acrylic/TiO_2 Waterborne Dispersions. *Crystals* **2016**, *6*, 136. [CrossRef]
58. Fujishima, A.; Rao, T.N.; Tryk, D.A. Titanium dioxide photocatalysis. *J. Photochem. Photobiol. C Photochem. Rev.* **2000**, *1*, 1–21. [CrossRef]
59. Blanchard, C.; Brooks, L.; Ebsworth-Mojica, K.; Didione, L.; Wucher, B.; Dewhurst, S.; Krysan, D.; Dunman, P.M.; Wozniak, R.A.F.; Fey, P.D. Zinc Pyrithione Improves the Antibacterial Activity of Silver Sulfadiazine Ointment. *mSphere* **2016**, *1*, 1–14. [CrossRef]
60. Dinning, A.J.; Al-Adham, I.S.; Eastwood, I.M.; Austin, P.; Collier, P.J. Pyrithione biocides as inhibitors of bacterial ATP synthesis. *J. Appl. Microbiol.* **1998**, *85*, 141–146. [CrossRef] [PubMed]
61. Reeder, N.L.; Xu, J.; Youngquist, R.S.; Schwartz, J.R.; Rust, R.C.; Saunders, C.W. The antifungal mechanism of action of zinc pyrithione. *Br. J. Dermatol.* **2011**, *165*, 9–12. [CrossRef] [PubMed]